Second Harmonic Exploitation for High-Efficiency Wireless Power Transfer Using Duplexing Rectenna

Sumin David Joseph, Yi Huang, *Senior Member, IEEE*, Shawn S. H. Hsu, *Member, IEEE*, Ahmed Alieldin, *Member, IEEE*, and Chaoyun Song, *Member, IEEE*

***Abstract*— In this article, a novel duplexing rectenna with harmonic feedback capability is proposed for efficient wireless power transfer (WPT) applications. The proposed duplexing rectenna can harvest the incoming radio frequency (RF) energy efficiently and also make use of an inherent harmonic signal, which is sent back to the RF transmitter (Tx) for positioning in order to guide the radiation patterns from Tx antenna array for optimum WPT. A novel duplexing dipole antenna is designed based on the top loading and capacitive gap effects. It is used to receive RF power at fundamental frequency 0.915 GHz and transmit the second harmonic signals at 1.83 GHz as a feedback. Experimental validation of a complete WPT system with beam-scanning capability has been carried out. It is shown that the fabricated rectifier has realized a maximum RF-dc conversion efficiency of 71% (at 15-dBm input power) and a measured peak second harmonic power of −1 dBm. Thus, the proposed duplexing rectenna can form a closed-loop system by providing its location information for efficient WPT applications.**

***Index Terms*— Antenna, duplexing antenna, harmonic feedback, rectenna, rectifier, second harmonic, wireless power transfer (WPT).**

I. Introduction

WIRELESS electronic devices have grown immensely over the last decades. The idea of wireless electronics is moving beyond networking people to sensors and devices, thus creating an "Internet of Things" (IoT) which enable these objects to collect and exchange data [1]. This exponential increase in wireless devices demands a method for effective power supply to realize self-sustainable operation. Wireless power transfer (WPT) is a promising technology to power these devices [2]. In a WPT system, the power from the transmitter (Tx) is wirelessly captured by a rectenna which can convert the incident radio frequency (RF) power into dc power for many sensing devices [3].

Manuscript received July 17, 2020; revised September 15, 2020 and October 21, 2020; accepted October 25, 2020. *(Corresponding authors: Yi Huang; Shawn S. H. Hsu.)*

Sumin David Joseph and Yi Huang are with the Department of Electrical Engineering and Electronics, University of Liverpool, Liverpool L69 3GJ, U.K. (e-mail: sumin.joseph@liverpool.ac.uk; yi.huang@liverpool.ac.uk).

Shawn S. H. Hsu is with the Department of Electrical Engineering, National Tsing Hua University, Hsinchu 300, Taiwan (e-mail: shhsu@ee.nthu.edu.tw).

Ahmed Alieldin is with The Egyptian Technical Research and Development Centre, Elsayeda Aisha, Cairo 11618, Egypt (e-mail: ahmed.alieldin@alexu.edu.eg).

Chaoyun Song is with the School of Engineering and Physical Sciences, Heriot-Watt University, Edinburgh EH14 4AS, U.K. (e-mail: c.song@hw.ac.uk).

Color versions of one or more figures in this article are available at https://doi.org/10.1109/TMTT.2020.3039604.

Digital Object Identifier 10.1109/TMTT.2020.3039604

For wireless energy harvesting (WEH) scenarios, ambient RF sources are taken into consideration [3], [4]. Conventionally, the rectenna for WEH and WPT is designed in a similar way, without considering the advantages of a dedicated RF source [5]. Therefore, the conventional rectennas for WEH and WPT can only offer a limited amount of dc power and normally do not have the location knowledge of the rectenna [3]–[5]. To direct the microwave energy beam toward the desired rectenna and to enhance the incident power level, several researchers proposed antenna arrays with beam steering capabilities [5]–[7]. Due to the use of antenna array for high gain performance, the radiation is very directive. Therefore, a slight misalignment can lead to a big drop in energy conversion efficiency and output dc power [8]. In this scenario, a feedback signal from the receiver (Rx) to the Tx can be used to overcome this problem [9]. However, it is challenging to create a passive and simple feedback signal from the Rx side where power is a critical issue. Some designs on wireless powered sensors combined with backscatter modulation have been reported in [10] and [11], these designs use two tones for energy harvesting and information transfer, respectively.

Few studies were carried out by researchers to investigate the relation between harmonic effects in rectifiers and output dc power [12], [13]. Furthermore, these works were mainly focused on harmonic terminations to suppress the generated harmonics and enhance rectifier performance. Another work attempted to recycle and harvest the harmonics for improving the power conversion efficiency of the rectifier by rerectifying the harmonics [14]. An energy harvesting passive UHF RFID relying on the exploitation of the power carried by the third harmonic signal generated by the RFID chip to provide dc power to an associated sensor while simultaneously communicating with the reader is reported in [15]. A retrodirective system utilizing second harmonic reradiation as pilot signal from a rectenna was presented in [16]. In [17], UHF multisine excitations of a battery-less RFID tag were utilized for recycling the unwanted harmonics generated by the rectifier nonlinear regime to build a fully passive UWB generator. Thus, a promising technology is to use harmonics generated by the rectifying element as a feedback signal from the Rx for providing the knowledge about the Rx node [18]–[20]. Couplers or separate antenna elements were employed in these designs to feedback the harmonic power [18]–[20].

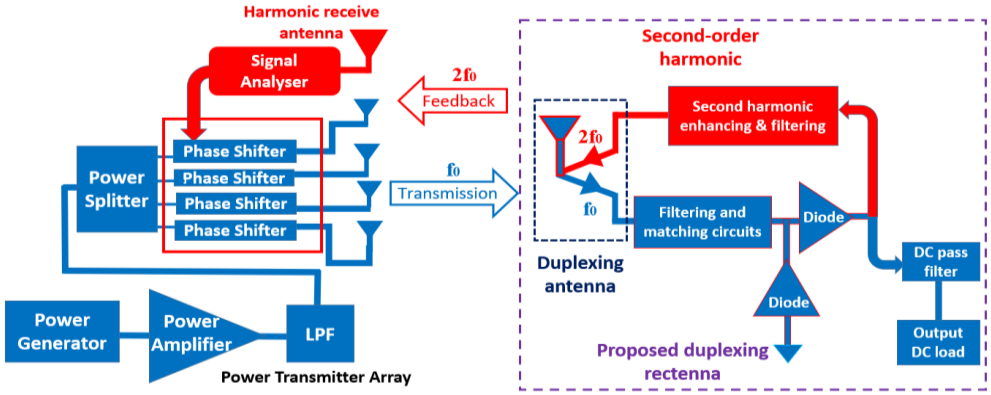

Fig. 1. Proposed duplexing rectenna system with harmonic feedback capability for localization in WPT.

In this article, we present the design of a novel duplexing rectenna with harmonic feedback capability for WPT applications and it offers the potential to track the Rx for effective and efficient WPT. Fig. 1 shows the proposed duplexing rectenna system with localization capability for WPT. At the WPT Tx side, the power from the microwave generator at the fundamental frequency (f_0) is amplified by a power amplifier. To reduce the effect of harmonics in the amplified signal, a low pass filter (LPF) is utilized. Then, a power splitter is employed to evenly allocate the power to the antenna array elements. A set of phase shifters is used to control the radiation direction. In the Rx side, a novel duplexing rectenna is designed to perform the WPT operation along with the feedback generation. One major novel contribution of this work is the duplexing antenna and harmonic feedback rectifier integration; to the best of the author's knowledge, such an integrated design has never been reported before. More specifically, one antenna element can perform both harmonic feedback and WPT functions simultaneously. Although the harmonic feedback rectifiers have been reported, the proposed rectifier has reported relatively high feedback power of -1 dBm. So, the proposed single antenna based rectenna can send feedback signals over a relatively long distance with a considerably high-power conversion efficiency. A harmonic receive antenna in the Tx side accepts the second harmonic signal ($2f_0$) from the duplexing antenna, based on which the maximum radiation direction can be determined. As the Tx antenna array has high gain and narrow beamwidth, the duplexing rectenna requires a wide beamwidth in horizontal angle for accepting the WPT power and to send the feedback even in angles for demonstrating the antenna misalignment property. Then by controlling the phase-shifters of array to the direction of maximum feedback power, targeted WPT becomes possible.

The rest of this article is structured as follows. Section II explains the design and operation principle of the proposed duplexing antenna. The measured results are also explained in this section, Section III describes the design and performance of the harmonic feedback rectifier. Then, experimental validation of the complete WPT system including antenna array and duplexing rectenna is performed in Section IV. Finally, conclusions are drawn in Section V emphasizing the achievements of this research and future work directions.

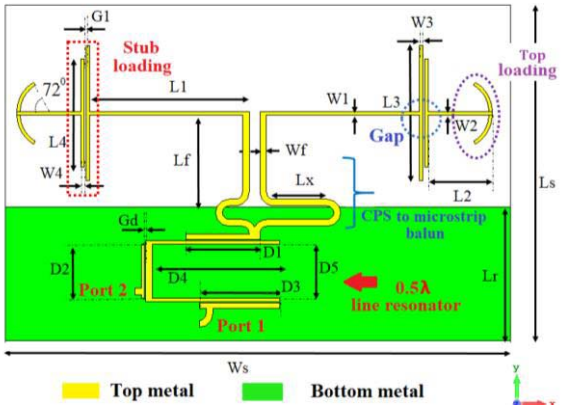

Fig. 2. Proposed duplexing antenna.

II. Duplexing Antenna

A. Antenna Structure

The geometry of the proposed duplexing antenna is depicted in Fig. 2. In order to demonstrate the viability of this novel idea, we should select f_0 and $2f_0$ ideally from the license-free ISM bands. Checking the ISM bands, we can see that 13.56 and 27.12 MHz, as well as 61.1 and 122 GHz are the ISM bands available for both f_0 and $2f_0$. However, in order to develop a demonstration system using a reasonably compact size and low loss, these frequencies are not selected on the basis of large wavelength (e.g., 13.56 MHz) and large attenuation (e.g., 61.1 GHz), at the end the ISM band frequency 0.915 GHz has been selected as the primary power transfer frequency for our optimized proof-of-concept prototype. Moreover, 915 MHz has been widely used for the studies and researches in WPT applications as reported in [13] and [18]. The proposed novel dipole antenna consists of a capacitive gap, a top loading, and stub loading structure at each pole to realize as a compact dual-band dipole antenna which is printed on a Rogers RO4350B substrate with a relative permittivity of 3.48 and thickness of 1.52 mm. The capacitive gaps aided to generate the dual-band resonances at f_0 and $2f_0$ frequencies and also to create similar radiation patterns in fundamental and harmonic bands. Moreover, the proposed dual-band antenna is coupled to a λ microstrip line resonator for the duplexing action. Port 1 is used to excite

TABLE I
PARAMETERS OF THE PROPOSED ANTENNA

Parameter	Value (mm)	Parameter	Value (mm)	Parameter	Value (mm)
L1	47.2	W1	0.8	Ar	25.4
L2	17	W2	0.5	Wr	1
L3	52	W3	1	Lf	37.2
L4	38	W4	1	Wf	2.5
Lm	7.5	Wm	9	G1	0.2
Lx	23	Wx	9	G2	0.2
D1	22	E1	1.6	D5	20
D2	19	E2	0.4	E5	1
D3	27	E3	1.5	Lr	43.3
D4	38	E4	0.5	Ls	114
Ws	150				

the fundamental mode for receiving the 0.915-GHz signals to perform the WPT. Harmonic feedback is transmitted back through port 2 at 1.83 GHz. All the physical dimensions of this antenna (after optimization to be discussed later) are tabulated in Table I.

B. Evolution of Dual-Band Antenna Design

Dipole antennas are widely used in rectenna designs due to its broad beamwidth and structure simplicity. The target in this work is to design a half-wavelength dipole antenna that resonates at 0.915 and 1.83 GHz for receiving RF power and sending feedback signals, respectively. The reason for choosing such frequencies is that the rectifier circuit generates a second harmonic signal which can be used for feedback radiation as will be discussed in detail in Section III.

The conventional center-fed dipole can only excite odd-order modes [21]. Thus, a conventional half-wavelength dipole at 0.915 GHz is not good as its second odd mode is at 2.745 GHz, a new design for these two frequencies is required. The proposed dual-band antenna is evolved from three reference antennas as shown in Fig. 3. Initially, the Ref 1 half-wavelength dipole at 0.61 GHz with a length of 202 mm is selected. The second odd mode frequency in this case is at 1.83 GHz. The second reference design is a dipole antenna with capacitive gaps as in Fig. 3. Each arm of the dipole is divided into two equal segments ($x1 = x2 = 50.5$ mm) by a gap width of 0.2 mm to provide a capacitive effect. The gap cuts off the flow of current and stores the electric field energy.

According to the capacitive reactance X_C, relationship with frequency as in [22]

$$X_c = 1/\omega C. \tag{1}$$

The capacitive gap reactance has much more influence on lower frequencies compared to higher frequencies. Furthermore, coupling becomes stronger with the decreasing gap width *G1*. Therefore, resonance of the fundamental frequency of Ref 2 antenna is shifted up to 0.915 GHz from the 0.61 GHz of Ref 1 design due to the capacitive gap effects as shown in Fig. 4. Fig. 4 represents the Smith chart showing the fundamental and harmonic resonances of the reference designs and proposed antenna. Fig. 5(a) clearly reveals the frequency shift of fundamental mode. The current distributions of the

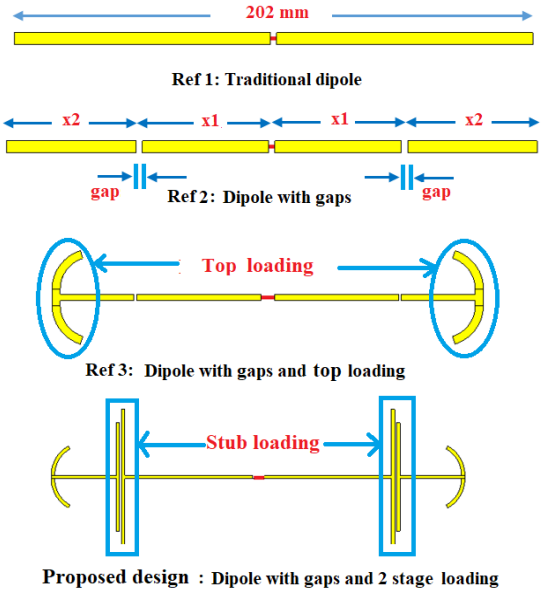

Fig. 3. Evolution of dual-band antenna design.

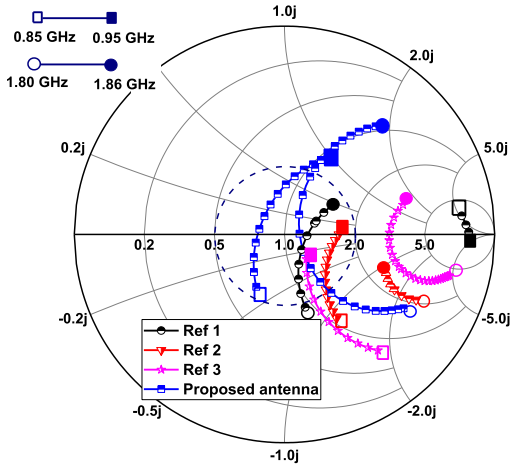

Fig. 4. Smith chart of the reference designs.

two resonant modes of the Ref 1 and 2 designs are given in Fig. 5(b). It can be confirmed that Ref 2 has the shifted fundamental mode at 0.915 GHz. Moreover, the capacitive gaps aided to enhance the central lobe and suppress the grating lobes in harmonic mode as depicted in Fig. 5(c). Therefore, the two resonant modes in Ref 2 has similar omnidirectional radiation pattern. However, the second resonance is slightly shifted away from 1.83-GHz frequency. Thus, top loading is introduced in the Ref 3 design, by making circular arcs at the end of each dipole arms. The circular arcs help to reduce the second segment length of each dipole arm, but it maximizes the volume of antenna in the "*kr*" sphere ("*k*" is the wavenumber and "*r*" is the radius of the smallest sphere that encloses the antenna) [23]. For a half-wavelength dipole

$$kr \approx 2\pi/\lambda \times \lambda/2 \approx \pi/2 \tag{2}$$

and the impedance bandwidth is far below the Wheeler–Chu limit [24]. Thus, the electrical size of the dipole can be reduced

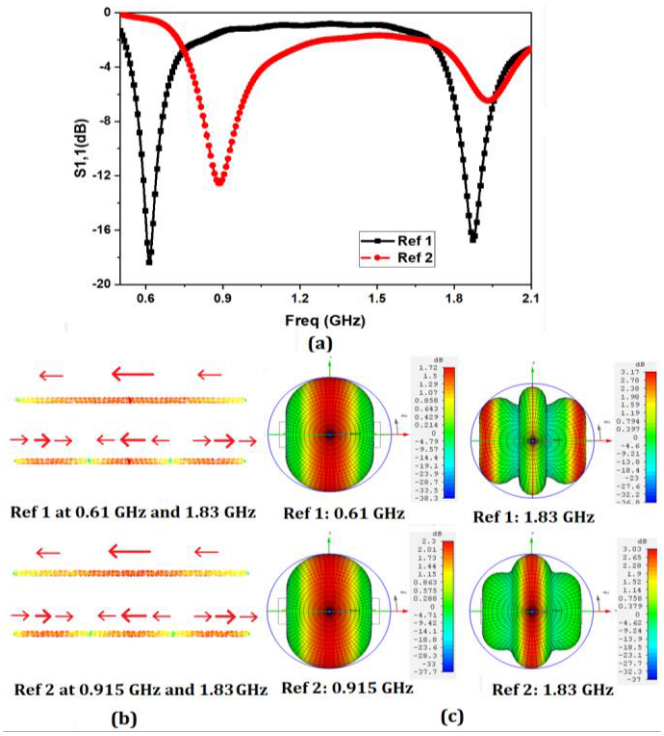

Fig. 5. (a) S1,1 of Ref 1 and Ref 2. (b) Surface current distribution of Ref 1 and Ref 2. (c) Radiation pattern of Ref 1 and Ref 2.

with a T-shaped top loading, while maintaining an impedance bandwidth similar to that of the $\lambda/2$ dipole. Hence, a kr of 1 is utilized to minimize the length of the antenna. Additionally, the resonance of the higher frequency band is shifted back to the 1.83 GHz due to the top loading. Unfortunately, this operation increases the real part of impedance due to the increase in overall length by the circular arcs. Further impedance matching is achieved in the proposed design by performing the stub loading in the gap region using the Smith chart analysis. Two stubs are used on either side of the gap in each dipole arm. This operation reduced the real part in the 1.83-GHz frequency band compared to Ref 3 and hence impedance matching becomes considerably simple. Dimensions of the stubs are optimized by analyzing the impedances in Smith chart with the aid of the Computer Simulation Technology (CST) software. Thus, an antenna is realized with pass bands at 0.915 and 1.83 GHz. To integrate the proposed antenna with microstrip rectifier, a coplanar strip (CPS) to microstrip balun is utilized. A truncated metal ground is used in the bottom plane of the substrate. This ground plane acts as a metal reflector and helps to obtain a beamwidth of around 180° in the H-plane with increased gains.

C. Duplexing Antenna Design

A duplexer is a device that allows the use of the single antenna by both Tx and Rx [25]. Some researchers have attempted to realize the antenna with duplexing properties [25], [26]. A simple architecture of duplexing dipole antenna is implemented by using a 0.5λ microstrip line resonator coupled to the feed of the dual-band antenna as shown in Fig. 2. Two resonances of the microstrip line are designed to work at 0.915 and 1.83 GHz. For receiving the 0.915-GHz

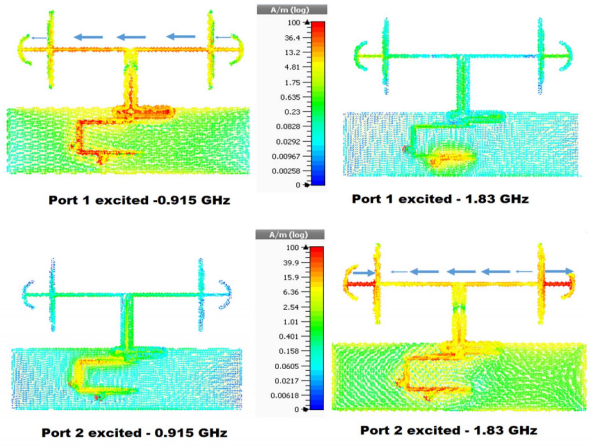

Fig. 6. Surface current distribution of duplexing antenna at different modes.

signal, a coupled port 1 is positioned at the end of 0.5λ microstrip line. Fine-tuning of the port placement is needed to achieve the maximum coupling of fundamental mode with a good consideration of harmonic signal isolation. Another coupled port is defined at the middle of the microstrip line for the harmonic signal. For the harmonic signal, 0.5λ microstrip line acts like a λ microstrip resonator. Therefore, at the line center the harmonic signal can be coupled with a zero-fundamental signal. The width of the line resonator and the coupled lines are adjusted to maximize the coupling of fundamental and harmonic signals with proper isolation. Thus, the simple 0.5λ microstrip line resonator can be used with dual-band antenna to form a duplexing antenna. Fig. 6 shows the surface current distribution of the duplexing antenna at different modes. Port 1 has the ability to excite the fundamental mode at 0.915 GHz and port 2 deals with the harmonic mode excitation. Surface current distribution clearly reveals that port 1 is completely isolated from the 1.83-GHz harmonic mode excitation and vice versa.

D. Duplexing Antenna Performance

To validate the predicted performance of this proposed duplexing antenna, a prototype was fabricated and measured. Fig. 7 shows the fabricated duplexing antenna. The proposed duplexing antenna has an overall dimension of 114 × 150 × 1.52 mm^3. Two SMA connectors are used to excite the two isolated bands of the fabricated antenna. Fig. 8 shows the simulated and measured S-parameter results of the duplexing antenna. A very good agreement between the measurements and simulations is achieved. The fundamental mode at 0.915 GHz is excited by port 1. The measured bandwidth of the duplexing antenna is 60 MHz which ranges from 0.895 to 0.955 GHz in the fundamental band. Correspondingly, port 2 can excite the harmonic mode with a bandwidth of 90 MHz which ranges from 1.815 to 1.905 GHz. The isolation between ports 1 and 2 in the fundamental band is around 13 dB. So, there is a very small leakage of WPT power at 0.915 GHz from the antenna to port 2. However, port 2 is in the output side of the rectifier and does not affect the performance and conversion efficiency of the rectifier. While in the harmonic

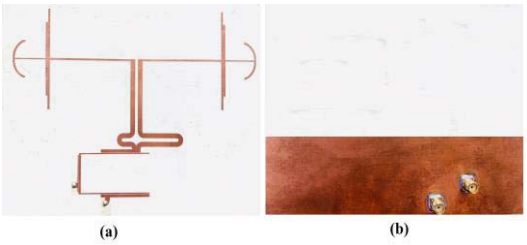

Fig. 7. Fabricated duplexing antenna. (a) Front view. (b) Back view.

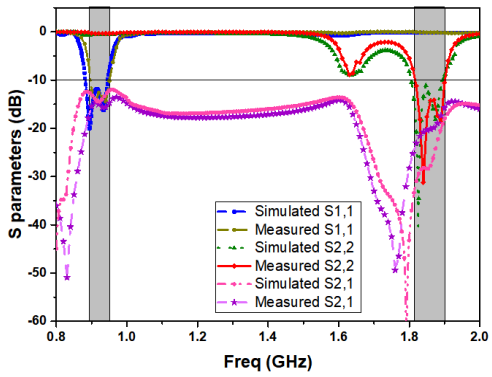

Fig. 8. Simulated and measured S parameters of the duplexing antenna.

band where power is crucial, the isolation is around 20 dB as shown in Fig. 8. Consequently, the power leakage is extremely small, and it does not affect the feedback power from the rectifier to antenna. The simulated 3-D radiation patterns of the proposed antenna with excitation at ports 1 and 2 are shown in Fig. 9(a). The half-power beamwidth of the duplexing antenna is 150.5° at 0.915 GHz and 177.6° at 1.83 GHz. Fig. 9(b) depicts the simulated efficiency of the antenna. The duplexing antenna has achieved a total efficiency of 88% in fundamental band and 84% in harmonic band. Fig. 9(c) shows the simulated and measured realized gains of the antenna. Maximum measured gain of 4.83 dBi was obtained at 0.9 GHz. Similarly, 4.68 dBi was measured at 1.833 GHz. It is interesting to note that both frequency bands have similar gains and radiation patterns with good isolation, making it as a good duplexing dipole antenna.

III. Harmonic Feedback Rectifier

A. Analysis of Harmonic Generation

A conventional rectenna block diagram is shown in Fig. 10. The RF power received from the antenna is converted to dc power by the rectifying circuit after passing through a filtering and matching network. A matching network (or bandpass filter) ensures that the antenna is matched to the rectifier and the harmonics generated by the rectifying element are not radiated back into the environment through the antenna [27]. Schottky diodes can be used as the rectifying element. An accurate model of the diode is required with a low threshold voltage, a high reverse breakdown voltage, a low junction resistance, and a low junction capacitance [28]. Current–voltage relationship through the nonlinear diode can be expressed as

$$I(V) = I_s\left(\exp^{\left(\frac{qV}{nkT}\right)} - 1\right) \tag{3}$$

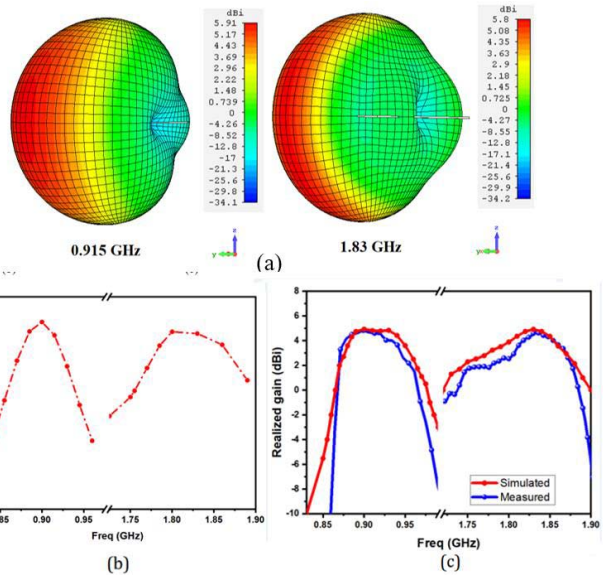

Fig. 9. (a) Simulated 3-D radiation patterns with excitation at ports 1 and 2, respectively. (b) Simulated efficiency. (c) Realized gain of duplexing antenna.

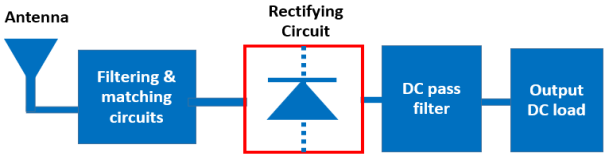

Fig. 10. Block diagram of a conventional rectifier.

where q is the charge of an electron, k is the Boltzmann's constant, T is the temperature, n is the ideality factor, and Is is the saturation current [14]. Let a sinusoidal signal input to the rectifier be

$$V = V_s\cos(\omega_0 t) \tag{4}$$

where V_s is the amplitude and ω_0 is the frequency of the input signal. The output response of a nonlinear diode rectifier can be modeled as a Taylor series in terms of input signal voltage as

$$V_0 = x_0 + x_1 V + x_2 V^2 + x_3 V^3 + \cdots \tag{5}$$

where $x_0, x_1, x_2, \ldots$ are the Taylor expansion coefficients [29]. For sinusoidal input in (4), Taylor series can be expanded as

$$V_0 = x_0 + x_1 V_s\cos(\omega_0 t) + x_2[V_s\cos(\omega_0 t)]^2 + x_3[V_s\cos(\omega_0 t)]^3 + \cdots \tag{6}$$

Since

$$\cos^2(\theta) = \frac{1}{2}(1 + \cos(2\theta)) \tag{7}$$

and

$$\cos^3(\theta) = \frac{3}{4}\cos(\theta) + \frac{1}{4}\cos(3\theta) \tag{8}$$

$$V_0 = x_0 + x_1 V_s\cos(\omega_0 t) + \frac{x_2}{2}V_s^2 + \frac{x_2}{2}V_s^2\cos(2\omega_0 t) + \frac{3x_3}{4}V_s^3\cos(\omega_0 t) + \frac{x_3}{4}V_s^3\cos(3\omega_0 t) + \cdots \tag{9}$$

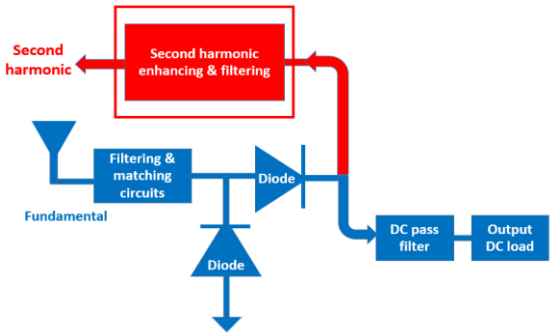

Fig. 11. Proposed block diagram of harmonic feedback rectifier.

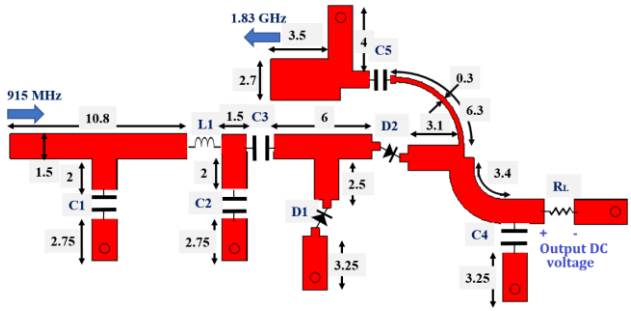

Fig. 12. Layout of harmonic feedback rectifier (dimensions in mm).

Thus, the output voltage contains dc rectified output and ac signals of frequency ω_0, $2\omega_0$, and $3\omega_0$ (as well as higher order harmonics), which are usually filtered out with a simple LPF. Moreover, the second and third order harmonics increases with increase in incident RF power. The second and third harmonics generated from the rectifier can be expressed as

$$V_{2\omega_0} = \frac{x_2}{2} V_s^2 \cos(2\omega_0 t) \tag{10}$$

$$V_{3\omega_0} = \frac{x_3}{4} V_s^3 \cos(3\omega_0 t). \tag{11}$$

In conventional rectenna design, a dc pass filter is used to obtain a ripple-free dc signal by suppressing the fundamental and harmonic frequencies from the rectified output. DC pass filter also has a key role in determining the output impedance for maximizing the dc power. An important concern in the design of feedback rectifier is to ensure the efficient operation of primary function, i.e., WPT. So, it is necessary to design the rectifier with high dc output power. Another essential consideration is to avoid the use of external power or a part of rectified dc power [18]. As (10) reveals that the second harmonic power increases with rectifier input power and has higher value than third harmonic, this work proposed a second harmonic feedback rectifier. Fig. 11 represents the proposed block diagram of the harmonic feedback rectifier. It demonstrates the RF to dc power rectification process and channeling the second harmonic from the rectifier output by enhancing and matching. A voltage doubler circuit is adopted for the design of this harmonic feedback rectifier. A second harmonic enhancing and filtering part is commenced from the output side of diodes, before the dc pass filter. The power of the second harmonic is very crucial as it acts as a feedback signal. Therefore, great care is needed to enhance and match the impedance to the output feedback port.

B. Harmonic Feedback Rectifier Design

A novel harmonic feedback rectifier is designed based on the above-mentioned requirements. The final layout is shown in Fig. 12. The harmonic feedback rectifier is designed to operate at 0.915 GHz which is printed on a Rogers RO4350B substrate with a relative permittivity of 3.48 and thickness of 1.52 mm. The design flow of the rectifier starts with determining the operating power level and expected output power. The operating input power for WPT application is typically 5–15 dBm [5]. Therefore, Schottky diode HSMS 2860B from Avago has been selected in the design. Moreover, the low junction capacitance and series resistance of this Schottky diode are also favorable for a high output dc power. In order to realize a high output voltage rectifier, a voltage doubler topology and a load resistance of 1000 Ω are selected. The large signal S-parameter (LSSP) and harmonic balance (HB) simulations are used to analyze the input impedance for impedance matching and conversion efficiency of the rectifier structure. A π-network of lumped components is used for filtering and matching of the fundamental frequency. It consists of two capacitors *C1*, *C2*, and an inductor *L1* with values 1.1 pF, 0.3 pF, and 15 nH, respectively, aiming to get the circuit matched at 0.915 GHz. Capacitors *C3* and *C4* have the function of storing the energy rectified by the rectifying elements *D1* and *D2*. Despite this energy storage function, *C3* works along with the input bandpass filter in the sense that it acts as a dc block. Similarly, *C4* in shunt with load resistor R_L acts as the output LPF with a $f_{\text{cut-off}}$, cutoff frequency $1/(2\pi\ R_L\ C4)$. Initially, both capacitors *C3* and *C4* are assigned to have a value of 20 pF to serve as a dc block filter. The chip capacitors and inductors are modeled using S-parameter files provided by Murata and Coil craft. After the rectifier performance is optimized for required output voltage and power, the next step is to design the harmonic extraction from the output of voltage doubler. The dc pass filter on the output side is critical in this design because it has an important role in determining the second harmonic power [17]. The output capacitor *C4* has a significant role in controlling the ripples and smoothing the output dc voltage. Normally *C4* with higher values can be directly used with R_L for realizing the output LPF to reduce the ripples in output voltage, by bypassing the harmonics to ground. But, in harmonic feedback rectifier the load resistance, R_L and *C4* can tune the power of harmonic signals. Variations of harmonic power and conversion efficiency as a function of capacitor *C4* are shown in Fig. 13. By providing an input power of 10 dBm to the rectifier, second harmonic power of −2 dBm can be observed with an output dc pass capacitor of 0.1 pF whereas third harmonic power is only −10 dBm which is about 8 dB smaller than the second harmonic. Furthermore, the propagation loss for higher modes is also more compared to lower frequencies. Therefore, second harmonic will be better as the feedback signal, as it is having more power.

In the designed rectifier, output capacitor has a very low impact on the input impedance of the rectifier. Moreover,

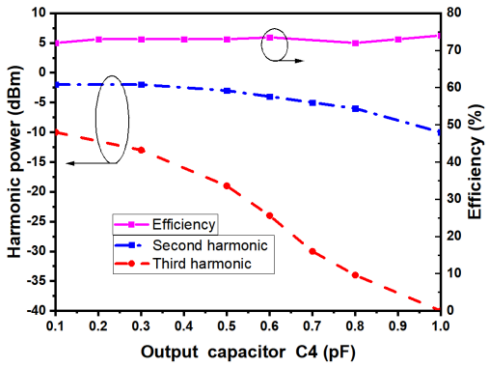

Fig. 13. Effect of output capacitor C4 in harmonic power and efficiency.

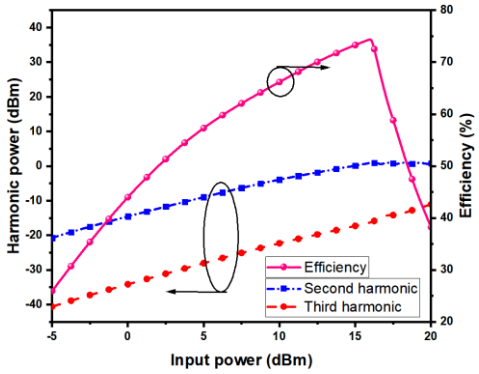

Fig. 14. Effect of harmonic power and conversion efficiency with respect to input power level.

TABLE II
CIRCUIT COMPONENTS USED IN THE RECTIFIER DESIGN

Component name	Nominal value	Part number and supplier
C1	1.1 pF chip capacitor	GRM0335C2A1R1CA01,Murata
C2	0.3 pF chip capacitor	GRM0335C2AR30BA01, Murata
C3	20 pF chip capacitor	GRM0335C2A200JA01, Murata
C4	0.5 pF chip capacitor	GRM0335C2AR50BA01, Murata
C5	1.5 pF chip capacitor	GRM0335C2A1R5CA01, Murata
L1	15 nH chip inductor	0402HP-15NX_E_, Coilcraft

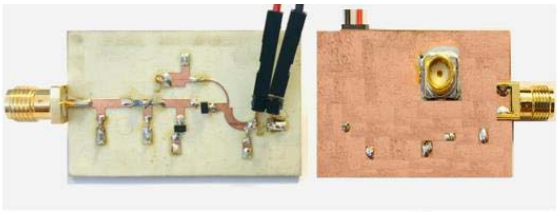

Fig. 15. Fabricated harmonic feedback rectifier. (a) Front view. (b) Back view.

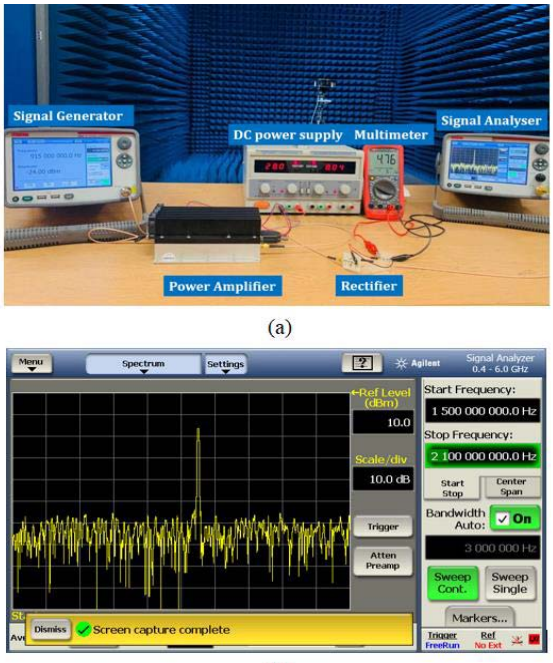

Fig. 16. (a) Experimental setup for rectifier measurement. (b) Harmonic spectrum at 12-dBm input power.

the rectifier is designed for moderate wide bandwidth. Thus, it is having relatively stable performance and good impedance matching for a change of *C4* from 0.1 to 1 pF. Efficiency is almost constant over 70% for different output dc pass capacitor values. So, it provides the opportunity to tune the capacitor *C4* for a better second harmonic power without disturbing the output power significantly. For realizing the harmonic feedback system, the second harmonic signal at the output of the rectifier is required to be enhanced and matched to the second port of the antenna. Capacitor *C5* has the functions of blocking the rectified dc and allowing the impedance matching of the second harmonic signal. Through proper tuning of the output capacitor *C4*, bypass capacitor *C5*, and the shorted stub length, the feedback signal is constructively directed to the harmonic port of the rectifier. These operations in the feedback signal branch do not impair the power conversion efficiency of the rectifier. In this design, after careful optimization, a 0.5-pF Murata capacitor is chosen as *C4* and 1.5 pF as *C5*. This value can provide a good conversion efficiency and second harmonic power with less ripples in the output dc voltage. The values and part numbers of the circuit components are given in Table II. Fig. 14 shows the effect of harmonic power and conversion efficiency as a function of input power. It can be clearly observed that the second and third harmonic power are increasing with input power and the second harmonic has higher power than third harmonic. Layout level simulations are performed using electromagnetic (EM) simulator momentum in ADS.

C. Harmonic Feedback Rectifier Performance

For evaluating the performance of harmonic feedback rectifier, a prototype is fabricated. A fundamental signal port is placed on the edge of the circuit board while the second connector for harmonic power is connected through the substrate. The overall dimension of harmonic feedback rectifier is 25 $\times$ 40 mm^2. The fabricated prototype is shown in Fig. 15. The experimental setup for rectifier measurement is illustrated in Fig. 16(a). The reflection coefficient of the designed rectifier is depicted in Fig. 17. The impedance

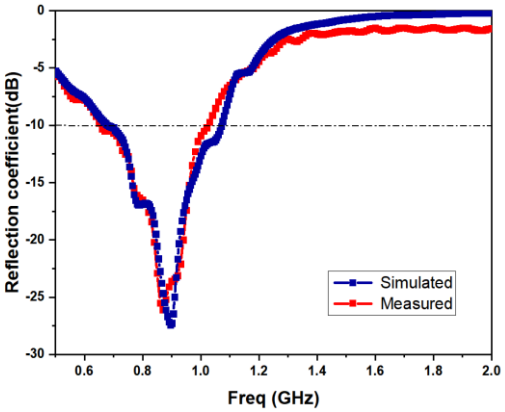

Fig. 17. Reflection coefficient of the harmonic feedback rectifier.

bandwidth of the harmonic feedback rectifier is 390 MHz which ranges from 680 to 1070 MHz at 5-dBm input power. A fundamental reflected power of −23 dBm is observed with an input power of 5 dBm at the input of rectifier. Reflected power of fundamental is 8 dB lower compared to the extracted second harmonic power (−15 dBm). A Keithley 2920 RF signal generator is used for signal generation at 0.915 GHz. The signal generator can provide a maximum output power of 13 dBm. Thus, a 40-dB power amplifier is used to amplify the signals for having complete access of the input power. The output power of the signal generator is varied from −41.5 to −19.5 dBm. A 3-dB attenuator is connected between the signal generator and power amplifier to protect the signal generator from any power surge and reflections. The input power from the power amplifier is estimated using a Keithley signal analyzer. After considering the 3-dB attenuator and the loss in cables, the power from the amplifier is estimated to be from −5 to 17 dBm. The output voltage and second harmonic power is measured by varying the input power. Second harmonic power is measured using the Keithley signal analyzer. Fig. 18(a) plots the output voltage variation with the input power. The maximum output voltage of 5.2 V is obtained at 17 dBm with a 1000-Ω load resistor. Second harmonic power is linearly increasing with input power and reaches at −1 dBm for an input power of 16 dBm as in Fig. 18(b). It can be observed that the simulated and measured conversion efficiency has a difference in low power region around −5 dBm. The measured one achieved only 12% while the simulated is around 25% at −5 dBm. A similar difference can be observed in the harmonic signal also. These differences in low input power are due to the inherent property of the diode to work well in high input power (5–15 dBm) and partially due to the impedance mismatch at lower input powers. Moreover, the parasitic behavior of the SMD components used in the circuit and the fabrication errors are also contributed to the slight differences in simulated and measured second harmonic power.

The rectifier RF to dc conversion efficiency is defined as

$$\eta = V_{\text{out}}^2 / R_L P_{\text{in}} \times 100\% \tag{12}$$

where V_{out} is the dc voltage across the load resistor R_L and P_{in} is the RF input power. Fig. 19 shows the simulated

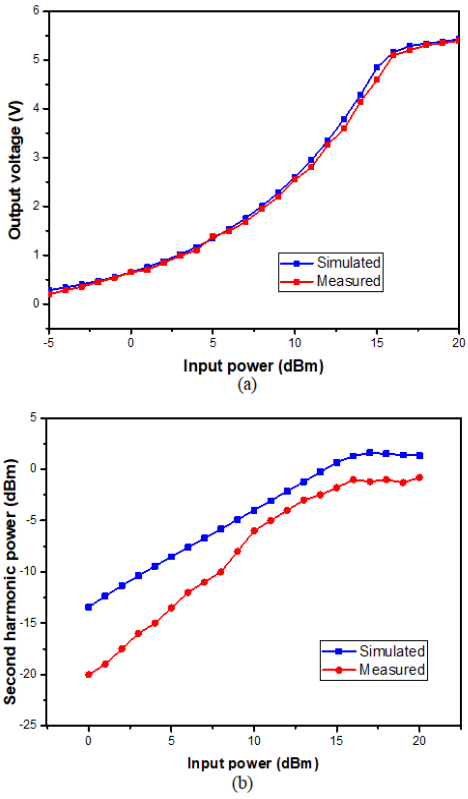

Fig. 18. Performance of rectifier as a function of input power. (a) Output voltage. (b) Second harmonic power.

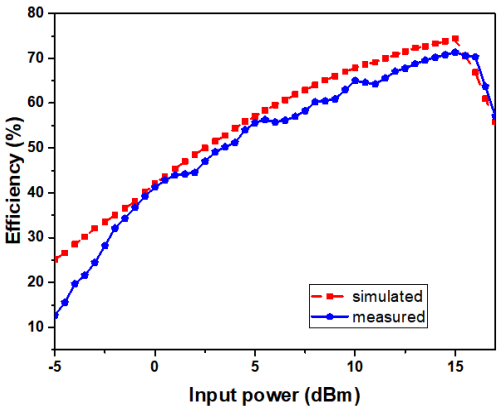

Fig. 19. RF to dc conversion efficiency versus input power.

and measured conversion efficiency for various input power. The harmonic feedback rectifier achieved a peak conversion efficiency of 71% at 15-dBm input power.

IV. Experimental Validation of Duplexing Rectenna and Comparisons

A prototype of the proposed rectenna is fabricated after careful cosimulation of the duplexing antenna and harmonic feedback rectifier. The rectenna is fabricated on a 1.52-mm Rogers RO4350B substrate as shown in Fig. 20. A four-element Tx antenna array is utilized with an overall width of 60 cm, to transmit the RF signal at 0.915 GHz. The array is fed by a four-way power divider which is fed by a 40-dB

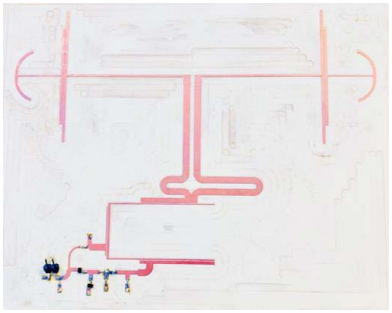

Fig. 20. Fabricated duplexing rectenna.

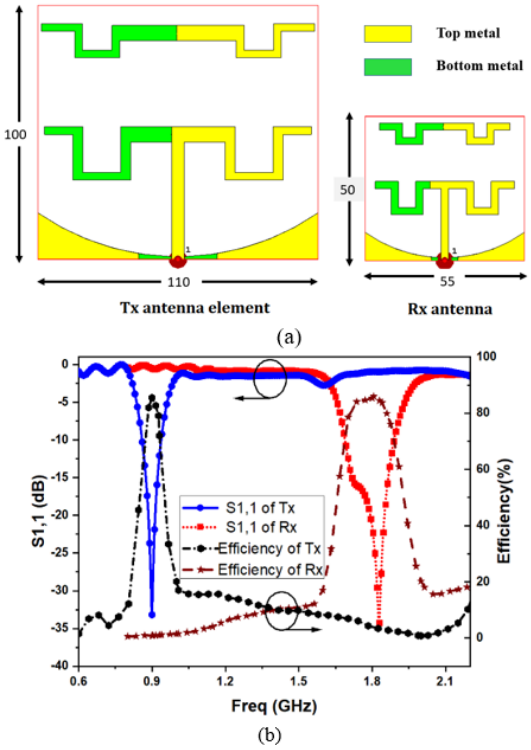

Fig. 21. (a) Layout of Tx antenna element and Rx antenna. (b) Reflection coefficient and efficiency of Tx and Rx antennas.

gain microwave GaN power amplifier, which amplifies the power generated by the signal generator. A harmonic feedback receives antenna (Rx) with a beamwidth of 155° is placed below the antenna array with a spacing of 15 cm to receive the second harmonic feedback signal from the duplexing rectenna at 1.83 GHz. Fig. 21(a) shows the layout of the Tx antenna array element and Rx antenna. Reflection coefficient and efficiency of Tx antenna element and Rx antenna are depicted in Fig. 21(b). The design is the same but for different frequencies. They are Yagi-Uda antennas with a meandered dipole and director, and curved reflector. Both antennas are fabricated on the FR4 substrate with a thickness of 1.52 mm. Simulated radiation patterns of the Tx antenna array (at various beam-scanning angles) and Rx antenna are shown in Fig. 22. The Tx antenna array has a gain of 12.5 dBi and the Rx antenna has a gain of 5.6 dBi.

As explained in Section III, a Keithley 2920 RF signal generator is utilized to generate the signal at 0.915 GHz,

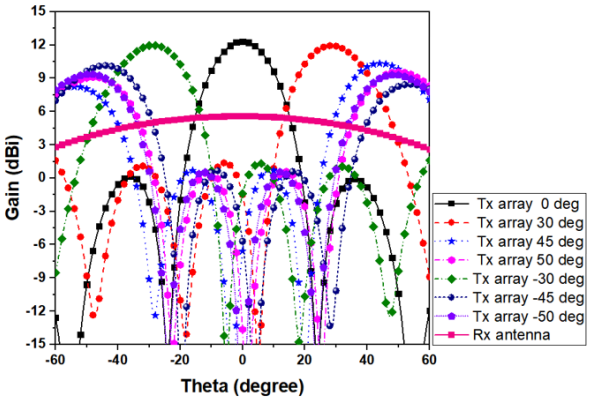

Fig. 22. Simulated radiation patterns of Tx antenna array (at various beam-scanning angles) and Rx antenna.

which fed to the power amplifier through a 3-dB attenuator. The power from the 40-dB power amplifier is estimated to be from 20 to 37 dBm. Then, the power is fed to the four-way power splitter (6-dB loss) through the LPF. A maximum second harmonic power of −43.5 dBm from the Tx array was observed in the Rx antenna, with a maximum input power of 29 dBm. Thus, an LPF VLF1000 having high attenuation in stopband is utilized to reduce the second harmonic power to a very low power around −86.5 dBm (noise floor). The cable losses in the Tx side and the insertion loss of LPF is estimated as 2 dB. Finally, the RF signal with power in the range of 12–29 dBm is fed to the Tx antenna array elements. Thus, the maximum EIRP is in the range of 41.5 dBm. In this measurement, distance R is set to be greater than 2.2 m, which satisfies the far-field condition at 0.915 GHz. The transmitted continuous wave high-power signals in these experiments are only used as a demonstration in laboratory conditions, rather than real world application. In real world scenario, to meet the EIRP safety levels, it is possible to use modulated signals or multicarrier signals to reduce the peak power levels. Fig. 23 illustrates the experimental setup for antenna alignment using second harmonic feedback signal. The dc output voltage is measured as a function of the received power derived by Friis' formula [30]. The power received in rectenna is therefore

$$P_r = P_t G_t G_r (\lambda_0/4\pi R)^2 \tag{13}$$

where P_t is the transmitted power, P_r is the received power, G_t is the Tx antenna array's gain, G_r is the Rx antenna gain, λ_0 is the free space wavelength, and R is the distance between the Tx and the rectenna. The received power in the duplexing rectenna is in the range of −12 to 7 dBm.

Fig. 24 describes the flowchart of operations for targeted WPT using feedback power. As observed in Section III, the output dc power from the rectenna is proportional to the received feedback signal, it is possible to evaluate antenna misalignment by analyzing the feedback signal power. Thus, this duplexing rectenna-based WPT system can determine the rectenna position by sweeping the Tx antenna array beam from −45° to 45° by controlling the phase shifters and analyzing the feedback power received by the Rx antenna at each beam

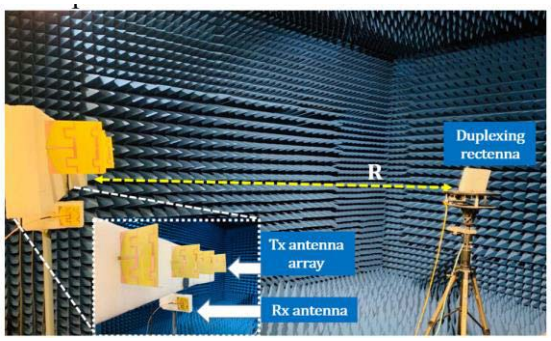

Fig. 23. Experimental setup for antenna alignment using second harmonic feedback signal.

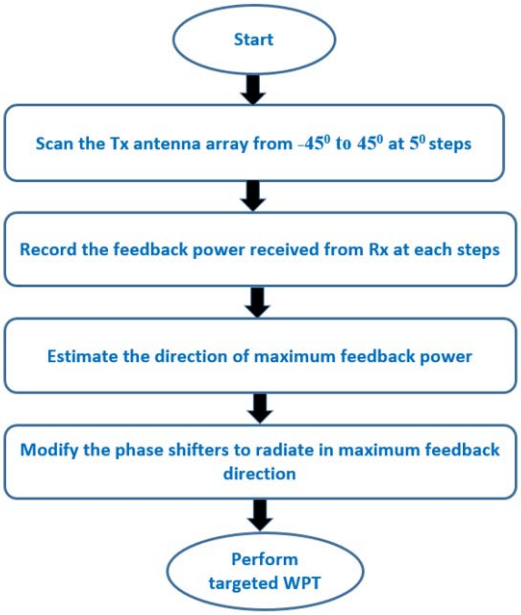

Fig. 24. Flowchart of operations for targeted WPT using feedback power.

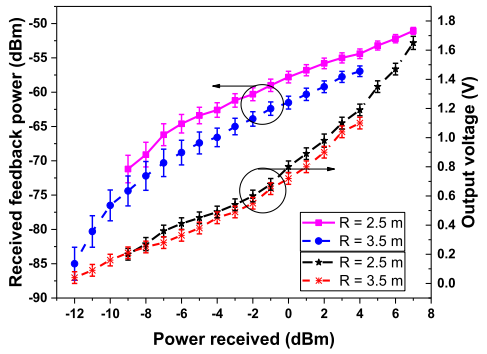

Fig. 25. Measured feedback power and dc voltage at $R = 2.5$ and 3.5 m.

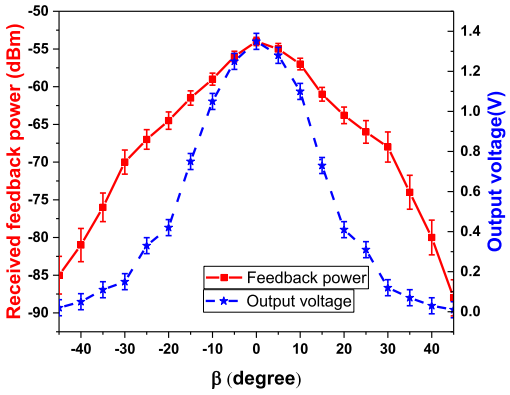

Fig. 26. Measured feedback power and dc voltage as a function of β.

positions. Initially, if the duplexing rectenna is misaligned with the Tx antenna array, the incident power on the rectenna will be low. Thus, a low feedback power will be recorded by the Rx antenna. Then, the Tx antenna array beam sweeping will record the corresponding relative feedback power at different beam directions. The peak value of the feedback power will be the position of the duplexing rectenna and hence the Tx antenna array and duplexing rectenna can align for maximum power transfer. Even though the Rx antenna is for the second harmonic, at the output of Rx antenna a maximum fundamental power of -36 dBm is observed. However, we have used the second harmonic power and neglected the fundamental power for the antenna alignment application by using a VBF-1840 bandpass filter centered around second harmonic. Fig. 24 shows the received second harmonic power and dc voltage measured at two different distances from the Tx antenna array and rectenna. The experiment was conducted multiple times to improve the accuracy of results and to analyze the uncertainties. The measured harmonic feedback powers and output dc voltages are shown in Figs. 25–27 with error bars. Output dc voltage has a small error while repeating the experiments for accuracy. However, at low received feedback power conditions slightly more fluctuations can be observed at the output of Rx antenna output. As the received power in rectenna is increasing, the received second harmonic power and output voltage are also increasing. The maximum output voltage measured at $R = 2.5$ m is 1.65 V, which is limited by the input power applied to the antenna array to protect the LPF power rating. Feedback power of -51.06 dBm is observed at $R = 2.5$ m, while at 3.5-m distance -56.95 dBm is measured.

For analyzing the feedback power from rectenna as a function of horizontal antenna misalignment angle (between the Tx antenna array and rectenna), the deviation angle β is varied in steps of 5°. R is kept as 2.5 m with a fixed transmitted power of 28 dBm fed to the Tx array elements. Fig. 26 shows the measured feedback power in Rx antenna and dc voltage from rectenna for β values ranging from $-45°$ to 45°. It can be observed that the maximum received second harmonic power -52 dBm and the maximum output voltage 1.4 V are achieved when β approaches 0°. Thus, the maximum feedback power from harmonic receive antenna and peak dc output voltage occur simultaneously at the angle corresponding to the position of the rectenna. To improve the robustness of the proposed system, a fixed phase shifter is used to tilt the antenna beam to 30° from the initial direction. Then, deviation angle β is varied to analyze the received feedback power at different rectenna positions. Fig. 27 shows the plot of measured feedback and dc voltage with a 30° phase shifter as a function of deviation angle β. It shows that the maximum second harmonic power as well as the output voltage can be

TABLE III
COMPARISON OF THE PROPOSED RECTENNA AND RELATED DESIGNS

Ref	[9]	[18]	[19]	[20]	**Proposed Rectenna**
Frequency (GHz)	2.45	0.915	2.45	2.6	**0.915**
Rectenna elements studied	Rectifier only	Rectifier and amplifier	Rectifier only	Rectifier only	**Duplexing rectenna (Rectifier+antenna)**
Extra antenna for harmonic feedback	Yes	No	No	Yes	**No**
Harmonic feedback type	Third - feedback	Second-feedback	Third - feedback	Second-feedback	Second- feedback
RF to DC conversion efficiency (%) at 10 dBm input power level	NA	30	59	NA	**65**
Harmonic power measured (dBm) at 10 dBm input power level	NA	-33	-26	NA	**-6**
Maximum measured conversion efficiency (%)	76	30	70.6	49.5	**71**
Maximum harmonic power measured in rectifier (dBm) at input power (dBm)	-21 at 7	-33 at 10	-12 at 20	-20 at 0	**-1 at 17**
Feedback power measured in transmitter side (dBm) at distance (m)	-53 at 0.5	-	-65 at 0.3	-49 at 1	**-51.06 at 2.5**
Distance coverage of feedback power	Medium	Low	Low	Medium	**High**

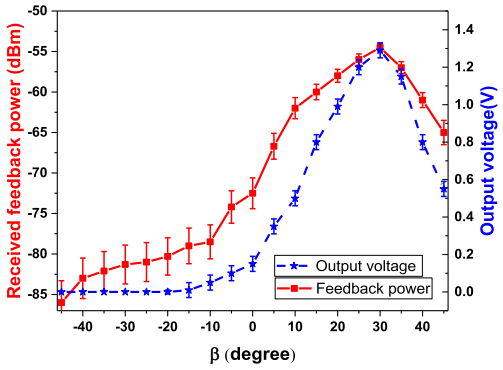

Fig. 27. Measured feedback power and dc voltage with a 30° phase shifter as a function of deviation angle β.

achieved when the deviation angle and the beam direction coincide. Harmonic feedback power of −54.5 dBm is observed from the harmonic receive antenna output while $\beta = 30°$. A maximum output voltage of 1.29 V is also observed in this specific β value. Therefore, it is possible to conclude that by scanning the Tx array and detecting the maximum feedback power received by the Rx antenna, the direction of rectenna can be determined. A comparison between our duplexing rectenna and some harmonic feedback rectenna designs is given in Table III.

Our integrated duplexing rectenna uses one antenna element to perform both harmonic feedback and WPT functions simultaneously. At a typical WPT power level of 10 dBm, the proposed duplexing rectenna can provide high RF to dc conversion efficiency with a reasonable feedback power. Moreover, the measured harmonic power of −1 dBm in rectifier is relatively high compared to other rectifier works. Thus, it is evident that our single antenna-based rectenna can send desired feedback signals over a relatively long distance with a considerably high-power conversion efficiency. Therefore, this duplexing antenna-based harmonic feedback rectenna can work as a standalone system which can provide a feedback signal for rectenna alignment to achieve efficient WPT.

V. CONCLUSION

A novel duplexing rectenna with a harmonic feedback capability has been proposed for efficient WPT applications with the antenna alignment. The proposed duplexing rectenna can efficiently convert the incident RF power at 0.915 GHz to dc and also send a reasonable harmonic signal back to the RF Tx at 1.83 GHz for tracking the position of rectenna to improve power transfer efficiency without the need of another antenna and Txs. The fabricated novel duplexing antenna exhibited dual-band operation with similar radiation pattern for RF power reception and sending the harmonic feedback signals simultaneously. A harmonic feedback rectifier with a maximum measured conversion efficiency of 71% and a peak second harmonic power of −1 dBm at 17 dBm has been proposed. The proposed duplexing rectenna is better than other published feedback rectenna designs in terms of the overall conversion efficiency as well as the harmonic feedback power at a typical WPT power level of 10 dBm. Experimental demonstration of rectenna alignment for optimum power transfer has been carried out by determining the maximum received feedback power. Thus, this complete WPT system based on a duplexing rectenna with feedback property is a very promising solution for future efficient WPT applications.

REFERENCES

[1] M. Zorzi, A. Gluhak, S. Lange, and A. Bassi, "From today's INTRAnet of things to a future Internet of Things: A wireless- and mobility-related view," *IEEE Wireless Commun.*, vol. 17, no. 6, pp. 44–51, Dec. 2010.

[2] M. Tabesh, N. Dolatsha, A. Arbabian, and A. M. Niknejad, "A power-harvesting pad-less millimeter-sized radio," *IEEE J. Solid-State Circuits*, vol. 50, no. 4, pp. 962–977, Apr. 2015.

[3] M. Piñuela, P. D. Mitcheson, and S. Lucyszyn, "Ambient RF energy harvesting in urban and semi-urban environments," *IEEE Trans. Microw. Theory Techn.*, vol. 61, no. 7, pp. 2715–2726, Jul. 2013.

[4] C. Song, Y. Huang, J. Zhou, J. Zhang, S. Yuan, and P. Carter, "A high-efficiency broadband rectenna for ambient wireless energy harvesting," *IEEE Trans. Antennas Propag.*, vol. 63, no. 8, pp. 3486–3495, Aug. 2015.

[5] S. Ladan, A. B. Guntupalli, and K. Wu, "A high-efficiency 24 GHz rectenna development towards millimeter-wave energy harvesting and wireless power transmission," *IEEE Trans. Circuits Syst. I, Reg. Papers*, vol. 61, no. 12, pp. 3358–3366, Dec. 2014.

[6] S. D. Joseph, Y. Huang, S. Hsu, M. Stanley, and C. Song, "A novel dual-polarized millimeter-wave antenna array with harmonic rejection for wireless power transmission," in *Proc. 12th Eur. Conf. Antennas Propag. (EuCAP)*, 2018, pp. 1–3.

[7] D. Masotti, A. Costanzo, M. Del Prete, and V. Rizzoli, "Time-modulation of linear arrays for real-time reconfigurable wireless power transmission," *IEEE Trans. Microw. Theory Techn.*, vol. 64, no. 2, pp. 331–342, Feb. 2016.

[8] Z. A. Pour, L. Shafai, and B. Tabachnick, "A practical approach to locate offset reflector focal point and antenna misalignment using vectorial representation of far-field radiation patterns," *IEEE Trans. Antennas Propag.*, vol. 62, no. 2, pp. 991–996, Feb. 2014.

[9] H. Zhang, Y.-X. Guo, S.-P. Gao, and W. Wu, "Wireless power transfer antenna alignment using third harmonic," *IEEE Microw. Wireless Compon. Lett.*, vol. 28, no. 6, pp. 536–538, Jun. 2018.

[10] S. N. Daskalakis, J. Kimionis, A. Collado, G. Goussetis, M. M. Tentzeris, and A. Georgiadis, "Ambient backscatters using FM broadcasting for low cost and low power wireless application," *IEEE Trans. Microw. Theory Techn.*, vol. 65, no. 2, pp. 5251–5262, Dec. 2017.

[11] T.-H. Lin, J. Bito, J. G. D. Hester, J. Kimionis, R. A. Bahr, and M. M. Tentzeris, "On-body long-range wireless backscattering sensing system using inkjet-/3-D-printed flexible ambient RF energy harvesters capable of simultaneous DC and harmonics generation," *IEEE Trans. Microw. Theory Techn.*, vol. 65, no. 12, pp. 5389–5400, Dec. 2017.

[12] M. Roberg, T. Reveyrand, I. Ramos, E. A. Falkenstein, and Z. Popovic, "High-efficiency harmonically terminated diode and transistor rectifiers," *IEEE Trans. Microw. Theory Techn.*, vol. 60, no. 12, pp. 4043–4052, Dec. 2012.

[13] J. Guo, H. Zhang, and X. Zhu, "Theoretical analysis of RF-DC conversion efficiency for class-F rectifiers," *IEEE Trans. Microw. Theory Techn.*, vol. 62, no. 4, pp. 977–985, Apr. 2014.

[14] S. Ladan and K. Wu, "Nonlinear modeling and harmonic recycling of millimeter-wave rectifier circuit," *IEEE Trans. Microw. Theory Techn.*, vol. 63, no. 3, pp. 937–944, Mar. 2015.

[15] D. Allane, G. A. Vera, Y. Duroc, R. Touhami, and S. Tedjini, "Harmonic power harvesting system for passive RFID sensor tags," *IEEE Trans. Microw. Theory Techn.*, vol. 64, no. 7, pp. 2347–2356, Jul. 2016.

[16] T. Mitani, S. Kawashima, and N. Shinohara, "Experimental study on a retrodirective system utilizing harmonic reradiation from rectenna," *IEICE Trans. Electron.*, vol. E102.C, no. 10, pp. 666–672, Oct. 2019.

[17] N. Decarli, M. Del Prete, D. Masotti, D. Dardari, and A. Costanzo, "High-accuracy localization of passive tags with multisine excitations," *IEEE Trans. Microw. Theory Techn.*, vol. 66, no. 12, pp. 5894–5908, Dec. 2018.

[18] C.-J. Peng, S.-F. Yang, A.-C. Huang, T.-H. Huang, P.-J. Chung, and F.-M. Wu, "Harmonic enhanced location detection technique for energy harvesting receiver with resonator coupling design," in *Proc. IEEE Wireless Power Transf. Conf. (WPTC)*, May 2017, pp. 1–3.

[19] H. Zhang, Y.-X. Guo, S.-P. Gao, Z. Zhong, and W. Wu, "Exploiting third harmonic of differential charge pump for wireless power transfer antenna alignment," *IEEE Microw. Wireless Compon. Lett.*, vol. 29, no. 1, pp. 71–73, Jan. 2019.

[20] T. Ngo and T. Yang, "Harmonic-recycling rectifier design for localization and power tuning," in *Proc. IEEE Wireless Power Transf. Conf. (WPTC)*, Montreal, QC, Canada, Jun. 2018, pp. 1–4.

[21] C. A. Balanis, *Antenna Theory: Analysis, and Design*, 3rd ed. Hoboken, NJ, USA: Wiley, 2005.

[22] R. Ludwig and P. Bretchko, *RF Circuit Design: Theory and Applications*. Englewood Cliffs, NJ, USA: Prentice-Hall, 2000, pp. 210–220.

[23] J. Chen, J. Ludwig, and S. Lim, "Design of a compact log-periodic dipole array using T-shaped top loadings," *IEEE Antennas Wireless Propag. Lett.*, vol. 16, pp. 1585–1588, 2017.

[24] D. F. Sievenpiper *et al.*, "Experimental validation of performance limits and design guidelines for small antennas," *IEEE Trans. Antennas Propag.*, vol. 60, no. 1, pp. 8–19, Jan. 2012.

[25] C.-X. Mao, S. Gao, Y. Wang, F. Qin, and Q.-X. Chu, "Compact highly integrated planar duplex antenna for wireless communications," *IEEE Trans. Microw. Theory Techn.*, vol. 64, no. 7, pp. 2006–2013, Jul. 2016.

[26] C.-X. Mao, S. Gao, and Y. Wang, "Dual-band full-duplex Tx/Rx antennas for vehicular communications," *IEEE Trans. Veh. Technol.*, vol. 67, no. 5, pp. 4059–4070, May 2018.

[27] R. Ibrahim *et al.*, "Novel design for a rectenna to collect pulse waves at 2.4 GHz," *IEEE Trans. Microw. Theory Techn.*, vol. 66, no. 1, pp. 357–365, Jan. 2018.

[28] C. R. Valenta and G. D. Durgin, "Harvesting wireless power: Survey of energy-harvester conversion efficiency in far-field wireless power transfer systems," *IEEE Microw. Mag.*, vol. 15, no. 4, pp. 108–120, Jun. 2014.

[29] D. M. Pozar, *Microwave Engineering*. Hoboken, NJ, USA: Wiley, 2009.

[30] Y.-H. Suh and K. Chang, "A high-efficiency dual-frequency rectenna for 2.45- and 5.8-GHz wireless power transmission," *IEEE Trans. Microw. Theory Techn.*, vol. 50, no. 7, pp. 1784–1789, Jul. 2002.

Sumin David Joseph received the B.Tech. degree (Hons.) in electronics and communication from the Cochin University of Science and Technology, Kochi, India, in 2012, and the M.Tech. degree (Hons.) in communication systems from the Visvesvaraya National Institute of Technology, Nagpur, India, in 2015.He is currently pursuing the dual Ph.D. degree in electrical engineering at the University of Liverpool, Liverpool, U.K., and National Tsing Hua University, Hsinchu, Taiwan.

He was a Lab Engineer under CoE with the Visvesvaraya National Institute of Technology, where he was involved in the projects of national importance. His research interests include self-biased circulators, mm-wave antenna arrays, rectifying antennas, rectifiers, wireless power transfer, and energy harvesting.

Mr. Joseph serves as a technical reviewer for leading academic journals and conferences.

Yi Huang (Senior Member, IEEE) received the B.Sc. degree in physics from Wuhan University, Wuhan, China, in 1984, the M.Sc. (Eng.) degree in microwave engineering from the Nanjing Research Institute of Electronics Technology (NRIET), Nanjing, China, in 1987, and the D.Phil. degree in communications from the University of Oxford, Oxford, U.K., in 1994.

Since 1987, he has been conducting research on wireless communications, applied electromagnetics, radar, and antennas. His experience includes three years spent with NRIET as a Radar Engineer and various periods with the University of Birmingham, Birmingham, U.K., the University of Oxford, and University of Essex, Colchester, U.K., as a Member of Research Staff. In 1994, he joined British Telecom Labs, lpswich, U.K., as a Research Fellow. In 1995, he joined the Department of Electrical Engineering and Electronics, University of Liverpool, Liverpool, U.K., where he is currently a Full Professor of wireless engineering, the Head of the High Frequency Engineering Group, and the Deputy Head of the Department of Electrical Engineering and Electronics. He has been a consultant to various companies. He has authored or coauthored more than 350 refereed articles in leading international journals and conference proceedings. He has authored *Antennas: From Theory to Practice* (Wiley, 2008) and *Reverberation Chambers: Theory and Applications to EMC and Antenna Measurements* (Wiley, 2016).

Prof. Huang is a Fellow of the IET and a Senior Fellow of the HEA. He has received many research grants from research councils, government agencies, charity, EU, and industry, and served on a number of national and international technical committees. He has been an editor, an associate editor, or a guest editor of five international journals. He has been a Keynote/Invited Speaker and an organizer of many conferences and workshops (e.g., WiCom 2006, 2010, IEEE iWAT2010, LAPC2012, and EuCAP2018). He is currently the Editor-in-Chief of *Wireless Engineering and Technology* and an Associate Editor of the IEEE ANTENNAS AND WIRELESS PROPAGATION LETTERS, and the Ireland Representative of the European Association of Antenna and Propagation (EurAAP).

Shawn S. H. Hsu (Member, IEEE) received the B.S. degree in electrical engineering from National Tsing Hua University, Hsinchu, Taiwan, in 1992, and the M.S. and Ph.D. degrees in electrical and computer engineering from the University of Michigan at Ann Arbor, Ann Arbor, MI, USA, in 1997 and 2003, respectively.

He is currently a Professor with the Department of Electrical Engineering, Institute of Electronics Engineering, National Tsing Hua University. He is involved in the design, fabrication, and modeling of high-frequency transistors and interconnects. His current research interests also include the design of monolithic microwave integrated circuits and RF integrated circuits using Si/III–V-based technologies, heterogeneous integration using system-in-package, and 3-D integrated circuit technology for high-speed wireless/optical communications and power electronics applications.

Ahmed Alieldin (Member, IEEE) received the B.Sc. degree in radar engineering from the Military Technical College, Cairo, Egypt, in 2005, the M.Sc. (Eng.) degree in antenna and microwave propagation from the University of Alexandria, Alexandria, Egypt, in 2013, and the Ph.D. degree in antennas and electromagnetics from the University of Liverpool, Liverpool, U.K., in 2019.

His academic research activities and Ph.D. were centered on antenna designing and measurements with an emphasis on mobile communication applications. In addition to work in academia, he also held various positions throughout more than 15 years working in the industry. He is currently a Senior RF Research Scientist with The Egyptian Technical Research and Development Centre, Cairo, Egypt, where he is involved in projects of national importance. He authored and coauthored many articles in leading international journals and conference proceedings. He has also filed a patent. His current research interests include novel textile antennas, multiple-input multiple-output antennas, base station antennas, satellite antennas, transparent antennas, high power antenna, phased-MIMO radar antennas and various types of RF and microwave circuits.

Dr. Alieldin served as a session chair in many international conferences and serves as a Technical Reviewer for leading academic journals and conferences.

Chaoyun Song (Member, IEEE) received the B.Eng., M.Sc., and Ph.D. degrees in electrical engineering and electronics from The University of Liverpool (UoL), Liverpool, U.K., in 2012, 2013, and 2017, respectively.

He was a Post-Doctoral Research Associate with UoL from 2017 to 2020. He is currently an Assistant Professor with the School of Engineering and Physical Sciences (EPS), Heriot Watt University, Edinburgh, U.K. He has published more than 60 articles (including 30 IEEE TRANSACTIONS) in peer-reviewed journals and conference proceedings. He has held two U.S. patents and two U.K. patents. His current research interests include wireless energy harvesting and wireless power transfer technologies, antennas and microwave circuits using novel materials, dielectric material and ionic liquids in RF applications, and metamaterials and metasurfaces in RF, energy harvesting, and sensing technologies.

Dr. Song was a recipient of many international awards, such as the BAE Systems Chairman's Award in 2017 for the innovation of next-generation global navigation satellite system antennas. In 2018, he received the highly commended award from the prestigious IET Innovation Awards over three categories—"Energy and Power," "Emerging Technologies," and "Young Innovators." He has been a regular Reviewer of more than 25 international journals, including *Nature Communications*, *Applied Physics Letters*, *Nano Energy*, and seven IEEE TRANSACTIONS and a Guest Editor for *Wireless Communications and Mobile Computing*.